Optimal integration of compression heat with regenerative steam Rankine cycles in oxy-combustion coal based power plants

Chao Fu[a,*], Rahul Anantharaman[b], Truls Gundersen[a]

[a] Department of Energy and Process Engineering, Norwegian University of Science and Technology, Trondheim, Norway
[b] SINTEF Energy Research, Trondheim, Norway

*Corresponding author. Tel.: +47 73592799; fax: +47 73593580; E-mail address: chao.fu@ ntnu.no

A b s t r a c t

The integration of process heat with regenerative steam Rankine cycles by preheating the boiler feedwater increases power generation from the steam turbines. In oxy-combustion coal based power plants, considerable compression heat from the air separation unit is available for such heat integration, however, there are at least two challenges: (1) how to integrate a heat stream with the steam cycle, and (2) how to optimize the compression scheme, accounting for the trade-off between compression work requirement and the turbine power output. This paper investigates the optimal integration of the air compression train in a cryogenic air separation unit with the regenerative steam cycle in an oxy-combustion coal based power plant using Mixed Integer Non-Linear Programming (MINLP). Two special cases (adiabatic compression and "isothermal" compression) are also investigated to compare with the optimization results. The study shows that such heat integration increases the thermal efficiency of the reference power plant by a maximum of 0.5-0.6% points. The heat integration is less attractive when the temperature difference of the heat transfer between the compressed gas and the boiler feedwater is larger than 40°C.

Keywords: optimization; steam Rankine cycle; regenerative preheating; heat integration; oxy-combustion

1 Introduction

In regenerative steam Rankine cycles, steam is extracted from the turbines at various pressure levels to preheat the boiler feedwater (BFW). This preheating process elevates the temperature at which the BFW receives heat in the boiler, thus increases the thermal efficiency of the power plant (defined as the ratio between the net work output from the cycle and the heat input to the cycle) [1]. In practice, a finite number of closed or open feedwater heaters (FWHs) are used for regenerative preheating. The temperature differences for the heat transfer between the extracted steam and the BFW should be minimized in order to reduce the irreversibilities. However, the capital cost increases. In modern pulverized coal based power plants, 6-9 FWHs are normally used in the steam cycle [2].

Alternatively, the BFW can be preheated by external heat sources. Steam extractions from turbines can thus be reduced or eliminated, resulting in increased power generation from the turbines. Such external heat sources could be solar [3], geothermal [4] or process heat [5]. One example of process heat is the waste heat from compression processes (compression heat) in oxy-combustion coal based power plants [6-8]. Compressors for CO_2 with a single-stage pressure ratio up to 10 have been developed by Ramgen Power Systems in order to upgrade the compression heat and integrate it with steam cycles [9]. In oxy-combustion processes, relatively purified O_2 is produced in an air separation unit (ASU) and then used for combustion, resulting in highly concentrated CO_2 in the flue gas after condensing the H_2O. Current air separation technologies for high volume O_2 supply are based on cryogenic air distillation [10]. When a

traditional double-column air separation scheme is applied for O_2 supply, the ASU causes a large thermal efficiency penalty of around 6 % points based on the higher heating value (HHV) [7]. According to the thermodynamic studies on the entire ASU [7, 11], around 40 % of the exergy losses in the ASU is caused by the compression of air from 1 bar to 5-6 bar, where around 54% of the compression losses are caused by compressor inefficiency and the remaining part is due to the (inter-stage and after-stage) cooling. A promising energy saving option is to utilize the corresponding compression heat for preheating BFW in the steam cycle.

When the compression heat is to be integrated with the steam cycle, the following two challenges should be addressed: (1) how to integrate a heat stream with the steam cycle, and (2) how to design the compression scheme tailored for this heat integration. The first challenge is normally solved by using Pinch Analysis [12]. A new heat balance in the feedwater heaters after heat integration is determined by drawing the Grand Composite Curve [5-7]. The second challenge is of particular interest since "isothermal" compression (multi-stage compression with interstage cooling to lower work consumption) may no longer be favorable. Complete or partial adiabatic compression can elevate the temperature of the available compression heat, and thus potentially reduce the extractions of higher pressure steam in the regenerative feedwater preheating process. Thus, there is a trade-off between the work consumption in the compression of air and additional power generation from the steam cycle due to the integration of compression heat. An optimization of the compression scheme is required. The available heat streams from the compression processes are unknown, increasing the complexity of solving the problem at hand. This paper presents a mathematical optimization study for the heat integration problem. The objective is to investigate the maximum improvement potential in thermal efficiency by integrating the compression heat from the ASU with the steam cycle. The influence of the temperature differences for heat transfer between the compressed gas and the BFW on the heat integration results is also investigated. The paper is an extension of the work by Fu et al. [13].

2 The reference steam cycle

A 571 MW (net) supercritical pulverized coal based oxy-combustion power plant [7] is illustrated in Figure 1. The entire power plant is modeled with the simulator Aspen Plus V7.3. The NBS/NRC steam tables are used for the steam cycle and the Peng-Robinson (PR) property method is used for the remaining processes. The thermal input from the coal is 1879 MW and thus the thermal efficiency is 30.4%. Around 95 mole% O_2 is produced from the cryogenic air separation unit (ASU) where the air feed is compressed to 5.6 bar. A major portion of the O_2 is used as oxidant in the combustor after being mixed with the recycled flue gas (RFG) that is used to control the combustor temperature. The heat of combustion is transferred to the steam cycle for power generation. A preheater is installed to further cool the flue gas against the mixture of the O_2 and the RFG. The NOx, the particulate matter and the SOx are removed in the DeNOx, ESP (Electrostatic Precipitator) and FGD (Flue Gas Desulfurization) units respectively. After desulfurization, a major portion (72%) of the flue gas is recycled while the remaining portion enters the compression and purification unit (CPU) where the CO_2 is purified to around 96 mole% and compressed to 150 bar.

A reference supercritical steam cycle [14] is shown in Figure 2 and the stream data is presented in Table A.1 (in Appendix). The high pressure (HP) steam is heated to 242 bar/600^{o}C with single reheat of the intermediate pressure (IP) steam to 45 bar/620^{o}C. The condenser pressure is 0.069 bar. The BFW is preheated in 4 closed FWHs (FWH1-4) in the lower pressure (LP) section, 1 open FWH (FWH5, i.e. the deaerator) and 3 FWHs (FWH6-8) in the higher pressure (HP) section. The mass flows and heat balances are obtained by process simulation. The heat contribution of the extracted steam in each FWH is determined by decomposing the heat loads as shown in Figure 3 [7]. In each FWH, the cold stream (represented by the bottom line) is the BFW. The hot streams (represented by the lines above the bottom line) are decomposed heat loads of the extracted steam at different pressure levels. They are actually

mixed in each FWH. External drain coolers (flash type) are used [15]. The condensate from each FWH is flashed to a lower pressure FWH (the deaerator is a special FWH) and condensed again at the lower saturation temperature. Thus the temperature of each extracted flow of steam does not decrease continuously. The extracted steam bypasses the subsequent turbine stages from its extraction point, thus reduces the power output from the turbines. The corresponding power reduction is determined on the basis of the following procedure:

(1) In the LP section of the BFW preheating (steam N24-27), the power reduction is equal to the additional power generated when the extracted steam passes through all the subsequent turbine stages from its extraction point.

(2) In the HP section below the reheating point (steam N18) and for the deaerator (steam N19), when the steam extraction is reduced, more steam passes through the subsequent turbine stages. However, the mass flow of BFW to be heated in the LP section and the deaerator increases and thus more steam (N19 and N24-27) is extracted. The power reduction caused by extraction of steam N18 and N19 is thus calculated by including two parts: (i) additional power generated from the turbines when assuming that the steam would pass through all the remaining turbine stages, and (ii) power reduction due to the preheating of increased BFW in the LP section and the deaerator.

(3) In the HP section above the reheating point (steam N15 and N16), when steam extractions are reduced, the reheating flow increases and thus additional heat (fuel) is consumed in the boiler area. This would change the entire power plant (more HP steam produced, more oxygen needed and more flue gas produced). A good approximation to find the net effect of reduced extraction for steam N15 and N16 is to assume that the extra heat (fuel) needed to handle increased reheating would produce power in a reference plant with the same thermal efficiency (30.4% for the reference oxy-combustion power plant according to [7]). Such power should be subtracted when determining the additional power generated by reducing the steam extraction. In addition, the mass flow of BFW in the LP section and the deaerator increases, similar to Case 2 above. Such influence should be taken into consideration when calculating the power reduction caused by extracting steam in the HP section.

For each extracted steam, the mass flow and the heat contribution to the preheating of BFW are obtained by process simulation. The corresponding power reduction and the specific power reduction, β, defined as power reduction per unit mass flow of extracted steam, are calculated according to the procedure described above. The results are shown in Table 1.

3 Integrating a heat stream with the steam cycle

Figure 4(a-c) shows 3 types of temperature profiles for FWHs in the reference steam cycle before heat integration. The lower curve in the figures is the one for the BFW, while the upper is the hot composite curve (mainly composed of the extracted steam according to Figure 3). The terminal temperature difference (TTD) refers to the difference between the saturation temperature of steam and the outlet temperature of the BFW [16]. When an external heat stream (k) is integrated with the steam cycle by preheating the BFW, the existing minimum temperature difference ($DT_{\min}$) for heat transfer between the extracted steam and the BFW in each FWH at the condensation temperature is assumed to be unchanged. The supply and target temperatures of the external heat stream are referred to as T_{kS} and T_{kT}. The corresponding modified temperatures are T'_{kS} and T'_{kT}, calculated as $T_{kS} - \Delta T_{\min}$ and $T_{kT} - \Delta T_{\min}$ respectively, where $\Delta T_{\min}$ is the minimum temperature difference for heat transfer between heat stream k and the BFW. When T'_{kS} is larger than the inlet temperature of the BFW in FWH r and smaller than that in the next higher pressure FWH, and T'_{kT} is smaller than the outlet temperature of BFW in FWH l and

larger than that in next lower pressure FWH, then heat stream k can always be integrated with FWHs between FWH l and FWH r.

The criteria for whether heat integration should be performed in FWHs r and l are listed in Table 2. The criteria are based on the assumption that the existing $DT_{\min}$ in each FWH is unchanged. For the LP FWHs, the steam extraction in the steam cycle is set such that the heating of BFW from T_2 to T_4 is done entirely by this extracted steam. Thus, steam extraction can be reduced only when heat stream k can be used in this range, as shown by Figure 4(d). Here, the part of the BFW that is heated by heat stream k has been removed. Heat integration reduces the heat demand in the range between T_2 and T_4 and thereby reduces steam extraction while maintaining the existing $DT_{\min}$. Figures 4(e-f) show that the integration of compression heat in the temperature range between T_1 and T_2 will not reduce the steam extraction in this FWH. If the steam extraction were to be reduced for this case, the resulting curves are shown in Figure 4(f). This would lead to unbalanced curves (missing heat supply to preheat a section of the BFW curve) and the $DT_{\min}$ is reduced at the pinch point T'_2. This heat can, however, be utilized in the next lower pressure FWH.

For LP FWHs, the pinch is hardly affected ($DT_{\min}$ at T_3 in Figure 4(a) almost equal to TTD) when heat is integrated in the range between T_2 and T_3. In contrast, for HP FWHs where TTD < 0 K, heat integration between T_2 and T_3 will affect the pinch as a reduction in steam extraction would move the pinch point to the right and thus reduce the $DT_{\min}$. The integration should thus not be performed in the temperature range between T_2 and T_3. The deaerator is a direct contact heat exchanger and the temperature difference for heat transfer can be as small as 0 K, thus steam extraction can be reduced by heat integration in the range between T_2 and T_4.

Table 3 lists complete ranges of T'_{kS} and T'_{kT} for determining whether a heat stream can be integrated with FWH i (i =1,2,3,4,5,6,7) in the reference steam cycle. The left square bracket "[" indicates the lower bound (the boundary value is included) and the right round bracket ")" indicates the upper bound (the boundary value is excluded). Note that for FWH6 and FWH7 in the HP section, the lower bound corresponds to temperature T_3 in Figure 4(b). For FWHs in the LP section, however, the lower bound corresponds to temperature T_2 in Figure 4(a). The same applies to the deaerator, i.e. FWH5 in Figure 4(c). For a given heat stream k with known T'_{kS} and T'_{kT}, the FWHs with highest and lowest pressures that can be integrated with stream k are identified based on Table 3. For example, when T'_{kS} =150°C and T'_{kT}=80°C, the FWH with highest pressure is FWH5 while the one with lowest pressure is FWH2, thus the heat stream can be utilized in FWHs 2-5. Note that FWH8 is not included in Table 3 since the maximum temperature of the compression heat ($T'_{\max}$) from the ASU can not reach the temperature range of FWH8.

A combination of temperature ranges j can now be defined with reference to the temperature ranges for the supply (g) and target (h) temperatures of heat stream (k). Since T_{kS} and T_{kT} in general are unknown variables as will be discussed in Section 4, the heat stream k can be located in any of these combined temperature ranges j listed in Table 3. Temperature range j is defined as: $a_g \le T'_{kS} < b_g$ (g =1,2,3,4,5,6,7) and $c_h \le T'_{kT} < d_h$ (h =1,2,3,4,5,6,7), where a_g, b_g, c_h and d_h are the lower and

upper bounds for T'_{kS} and T'_{kT} listed in Table 3. The index for the combined temperature range j is thus a function of the indexes for the ranges of supply and target temperatures: $j = h + \sum_{t=1}^{g-1} t$, where t is an integer variable, e.g. for the temperature range: $83.7 \le T'_{kS} < 106.2$ and $64.9 \le T'_{kT} < 83.7$, g =3, h =2, thus j is calculated to be 5. Once heat stream k is located in the temperature range j and used to preheat the BFW in FWH i, the new heat contribution from the extracted steam in this FWH, $\dot{Q}_{i,j,k}^{steam,new}$, is calculated by Eq. (1).

$$\dot{Q}_i^{BFW} = \dot{Q}_{i,j,k}^{steam,new} + \dot{Q}_{i,j,k} + \dot{Q}_i^{others} \tag{1}$$

where $\dot{Q}_i^{BFW}$ is the heat demand for preheating BFW in FWH i, $\dot{Q}_{i,j,k}$ is the heat contribution from heat stream k, and $\dot{Q}_i^{others}$ is the sum of heat contributions from other heat streams such as steam condensates from higher pressure FWHs (depending on the heat integration) and from other applications (such as steam sealing and pre-purification both in the ASU and the CO_2 compression and purification unit, CPU [7], see streams N28, N_{ASUb} and N_{CPUb} in Figure 2). According to Eq. (1), $\dot{Q}_{i,j,k}^{steam,new}$ can be negative when the amount of available heat ($\dot{Q}_{i,j,k}$) is too large, thus $\dot{Q}_{i,j,k}^{steam,new}$ must be constrained to be non-negative. The new mass flow of extracted steam, $\dot{m}_{i,j,k}^{steam,new}$, is calculated by Eq. (2).

$$\dot{m}_{i,j,k}^{steam,new} = \dot{m}_i^{steam} \times (\dot{Q}_{i,j,k}^{steam,new} / \dot{Q}_i^{steam}) \tag{2}$$

where $\dot{m}_i^{steam}$ and $\dot{Q}_i^{steam}$ are the mass flow and heat contribution of the steam extracted in FWH i in the case of no heat integration. Binary variables $y_{j,k}$ are introduced and $y_{j,k}$ =1 indicates that heat stream k is located in temperature range j, thus the new mass flow of extracted steam for FWH i after integrating heat stream k is determined by Eq. (3).

$$\dot{m}_{i,k}^{steam,new} = \sum_j (y_{j,k} \times \dot{m}_{i,j,k}^{steam,new}) \tag{3}$$

Binary variables are introduced to indicate whether the inequalities ($a_g \le T'_{kS} < b_g$ and $c_h \le T'_{kT} < d_h$) hold or do not hold [17], as shown by Eqs. (4a-d) and (5a-d):

$$m_g^L \times (1 - \lambda_{g,k}^L) - (T'_{kS} - a_g) \le 0 \tag{4a}$$

$$(T'_{kS} - a_g + \varepsilon_g^L) - (M_g^L + \varepsilon_g^L) \times \lambda_{g,k}^L \le 0 \tag{4b}$$

$$(T'_{kS} - b_g + \varepsilon_g^U \times \lambda_{g,k}^U) - M_g^U \times (1 - \lambda_{g,k}^U) \le 0 \tag{4c}$$

$$m_g^U \times \lambda_{g,k}^U - (T'_{kS} - b_g) \le 0 \tag{4d}$$

$$n_h^L \times (1-\mu_{h,k}^L) - (T'_{kT} - c_h) \le 0 \quad (5a)$$

$$(T'_{kT} - c_h + \sigma_h^L) - (N_h^L + \sigma_h^L) \times \mu_{h,k}^L \le 0 \quad (5b)$$

$$(T'_{kT} - d_h + \sigma_h^U \times \mu_{h,k}^U) - N_h^U \times (1-\mu_{h,k}^U) \le 0 \quad (5c)$$

$$n_h^U \times \mu_{h,k}^U - (T'_{kT} - d_h) \le 0 \quad (5d)$$

where m_g^L and M_g^L are the lower and upper bounds respectively for the expression $T'_{kS} - a_g$, $\lambda_{g,k}^L$ is a binary variable for indicating whether $T'_{kS} \ge a_g$ holds ($\lambda_{g,k}^L = 1$), ε_g^L is a small tolerance value beyond which the constraint $T'_{kS} \ge a_g$ is regarded to be broken. Similarly, m_g^U, M_g^U, n_h^L, N_h^L, n_h^U and N_h^U are lower and upper bounds, $\lambda_{g,k}^U$, $\mu_{h,k}^L$ and $\mu_{h,k}^U$ are binary variables, and ε_g^U, σ_h^L and σ_h^U are small tolerance values for T'_{kS} vs. b_g, T'_{kT} vs. c_h and T'_{kS} vs. d_h. These parameters are used to ensure that the binary variables act as indicators for the inequalities: $a_g \le T'_{kS} < b_g$ and $c_h \le T'_{kT} < d_h$. Thus, when temperature range j (a function of g and h) is selected, the binary variables $\lambda_{g,k}^L$, $\lambda_{g,k}^U$, $\mu_{h,k}^L$ and $\mu_{h,k}^U$ are all equal to 1, i.e. $\lambda_{g,k}^L \times \lambda_{g,k}^U \times \mu_{h,k}^L \times \mu_{h,k}^U = 1$, which is made linear by Eqs. (6a-e).

$$y_{j,k} \le \lambda_{g,k}^L \quad (6a)$$

$$y_{j,k} \le \lambda_{g,k}^U \quad (6b)$$

$$y_{j,k} \le \mu_{h,k}^L \quad (6c)$$

$$y_{j,k} \le \mu_{h,k}^U \quad (6d)$$

$$y_{j,k} \ge \lambda_{g,k}^L + \lambda_{g,k}^U + \mu_{h,k}^L + \mu_{h,k}^U - 3 \quad (6e)$$

4 The compression model

Figure 5 shows the scheme for compressing air from atmospheric pressure (1.01 bar) to the final desired pressure (p_F =5.6 bar is used in this study). Three compression stages are shown (more than 3 stages are not practical due to the pressure ratio). After each compression stage, the air is first cooled by the BFW and then cooled by cooling water (CW) in water coolers. The pressure drops in heat exchangers are neglected. Each compression stage is indexed with k ($k = 1,2,3$). For compression stage k, the outlet pressure p_k, the starting temperature T_{kS} and target temperature T_{kT} for heat integration, as well as the final temperature after water cooling T_{kF} are variables to be optimized. Since p_1, p_2 and p_3 may be equal to each other, the actual number of compression stages can be one (complete adiabatic compression), two (partial adiabatic compression) or three (an approximation to "isothermal" compression if the pressure

ratios are equal and water cooling is used after each stage).

4.1. Thermodynamic model

For cryogenic air separation processes, the Peng-Robinson (PR) or Redlich-Kwong-Soave (RKS) equation of state (EOS) are commonly applied for modeling [18]. The heat integration study requires the modelling of the air compression process. Both the PR and the ideal gas model have been tested with the simulator Aspen Plus V7.3 to model the isentropic compression process of ambient air (1 bar and 25ºC used here). The temperature and specific enthalpy after compression are shown in Table 4. The relative differences for temperature and enthalpy are limited to 0.05% and 0.5% respectively; thus the ideal gas model is used for simplification.

4.2. Objective function

The objective is to minimize the modified compression work $\dot{W}'$, defined as the total air compression work $(\dot{W}_1+\dot{W}_2+\dot{W}_3)$ minus the additional power generated from the steam turbines due to heat integration. The problem is formulated as an MINLP model and consists of Eqs. (7a-j) in addition to Eqs. (1-6), (8a-c) and (9a-c):

$$\min \quad \dot{W}' = \sum_{k=1}^{3}(\dot{W}_k - \dot{W}_{\dot{Q}_k}) \tag{7a}$$

$$s.t. \quad \dot{W}_k = \dot{m}_{air} \times \overline{c}_p \times (T_{kS} - T_{(k-1)F}) \tag{7b}$$

$$T_{kS} = T_{(k-1)F} + (T_{(k-1)F} + 273.15) \times (\alpha_k{}^{(\gamma-1)/\gamma} - 1) / \eta \tag{7c}$$

$$\dot{Q}_k = \dot{m}_{air} \times \overline{c}_p \times (T_{kS} - T_{kT}) \tag{7d}$$

$$\dot{W}_{\dot{Q}_k} = \sum_i [(\dot{m}_i^{steam} - \dot{m}_{i,k}^{steam,new}) \times \beta_i] \tag{7e}$$

$$\prod_{k=1}^{3} \alpha_k = 5.54 \tag{7f}$$

$$\alpha_k \geq 1 \tag{7g}$$

$$T_{kS} \geq T_{kT} \geq T_{kF} \tag{7h}$$

$$T_{0F} = T_0 \tag{7i}$$

$$T_{3F} = T_0 + 10^{\circ}\mathrm{C} \tag{7j}$$

where (i) $\dot{W}_k$ is the corresponding compression work for compression stage k, (ii) $\dot{Q}_k$ is the heat (with supply and target temperatures, T_{kS} and T_{kT}) transferred to the BFW and $\dot{W}_{\dot{Q}_k}$ is the additional power generated from the steam turbines due to the integration of heat from stream k, (iii) T_{kF} is the final temperature after water cooling and T_{0F} is the ambient temperature, (iv) $\dot{m}_{air}$, $\overline{c}_p$ and γ are the mass

flowrate, mean specific heat capacity and the specific heat capacity ratio of the air. The following values are used in this study: $\dot{m}_{air}$ =627.29 kg/s, $\overline{c}_p$ =1.02 kJ/(kg·K), γ =1.39, (v) α_k is the compression ratio for compression stage k, and (vi) η is the isentropic compressor efficiency.

The following explanations are given for Eqs. (7a-j): (7a) defines the objective function (minimizing the modified compression work), (7b) describes the calculation of compression work for each stage, (7c) describes the calculation of the supply temperature as the outlet temperature from a compressor with given isentropic efficiency, (7d) describes the amount of heat transferred to the steam cycle, (7e) describes the calculation of $\dot{W}_{\dot{Q}_k}$, where $\dot{m}_i^{steam}$, $\dot{m}_{i,k}^{steam,new}$ and β_i are described in Sections 2 and 3, (7f) puts a constraint on the total compression ratio (the final pressure is 5.6 bar), (7g) puts a limit on the compression ratio to avoid expansion being considered, (7h) ensures that the air is cooled after each compression stage, (7i) assigns a value to T_{0F}, and (7j) fixes the final temperature of the air from the water cooler to be 35ºC (cooling water temperature is assumed to be T_0 =25ºC and the temperature difference for heat transfer in the water cooler is 10ºC).

The compression process is modeled as a superstructure (Figure 5) to indicate that each of the compression stages may be selected or not. If a stage (k) is not selected, there is no compression heat to be removed from that stage, and the value of T_{kF} is either equal to $T_{(k-1)F}$ or T_0 (if $k=1$). When a stage is selected and if cooling water is used to remove the compression heat, then $T_{kF} \geq T_0 + 10^{\circ}\mathrm{C} = 35^{\circ}\mathrm{C}$. Eqs. (8a-c) describe the two situations when compression heat from stage k is removed by cooling water (binary variable $\omega_k = 1$) or is not ($\omega_k = 0$).

$$T_{kF} \geq 35 \times \omega_k + (1-\omega_k) \times T_0 \tag{8a}$$

$$T_{kT} - T_{kF} - X_k \times \omega_k \leq 0 \tag{8b}$$

$$T_{kT} - T_{kF} - \rho_k \times \omega_k \geq 0 \tag{8c}$$

where X_k is the maximum value of $T_{kT} - T_{kF}$, equal to $T'_{\max} + \Delta T_{\min} - T_0$ and ρ_k is a small tolerance value beyond which the constraint $T_{kT} - T_{kF} \geq 0$ is regarded to be broken. Eqs. (8b-c) forces ω_k to be 1 or 0 depending on whether $T_{kT} > T_{kF}$ or $T_{kT} = T_{kF}$ respectively. Eq. (7h) does not allow $T_{kT} < T_{kF}$.

Similarly, Eqs. (9a-c) describe the two situations when compression heat is integrated with the steam cycle (binary variable $\pi_k = 1$, $T_{kS} > T_{kT}$ and $T_{kT} \geq 42.7^{\circ}\mathrm{C} + \Delta T_{\min}$), and when compression heat is not integrated ($\pi_k = 0$, $T_{kS} = T_{kT}$ and $T_{kT} \geq T_0$). Here, $42.7^{\circ}\mathrm{C} + \Delta T_{\min}$ is the lowest temperature that the air can be cooled to by the BFW according to Table 3.

$$T_{kT} \geq (42.7 + \Delta T_{\min}) \times \pi_k + (1-\pi_k) \times T_0 \tag{9a}$$

$$T_{kS} - T_{kT} - Y_k \times \pi_k \leq 0 \tag{9b}$$

$$T_{kS} - T_{kT} - \xi_k \times \pi_k \geq 0 \tag{9c}$$

where Y_k is the maximum value of $T_{kS} - T_{kT}$, equal to $T'_{\max} + \Delta T_{\min} - T_0$, and ξ_k is a small tolerance value beyond which the constraint $T_{kS} - T_{kT} \geq 0$ is regarded to be broken.

5 Results and discussion

Two special cases are studied: one-stage complete adiabatic compression and three-stage "isothermal" compression (with equal pressure ratio). The results are used for estimating bounds when the optimization model is solved. The MINLP model contains 174 binary variables and is solved by Baron in GAMS 23.7 [19]. The running time is limited to 100,000 s (around 28 hours), since the best solution is found early in the search, and the rest of the time is spent to prove global optimality of the best available solution.

5.1. Performance of the heat integration

The results from the two special case studies (adiabatic and "isothermal") and the MINLP model solution are presented in Figure 6. Two isentropic compressor efficiencies have been used: 0.8 (solid curves) and 0.85 (dashed curves). The temperature difference for heat transfer (assumed to be the same for the entire heat transfer process) between the compression heat and the BFW is also investigated to find reasonable values for such heat integration. The thermal input of the oxy-combustion power plant is 1879 MW_{th} and the actual work consumption for the ASU ("isothermal" compression with an isentropic efficiency of 0.8) is about 127.8 MWe [7] (used as a reference value, almost equal to the value on the curve for "isothermal" compression with a temperature difference of 50°C). Detailed operating parameters for the optimized compression scheme are presented in Table A.2 (in Appendix).

From Figure 6 it can be observed that: (1) in the case of "isothermal" compression (isentropic efficiency = 0.8 and temperature difference = 10°C), heat integration increases total power output by 8.2 MWe (the thermal efficiency thus increases by 0.4 % points on HHV basis); (2) adiabatic compression saves more power compared to "isothermal" compression when the temperature difference is less than 50°C; (3) the maximum improvement in thermal efficiency by heat integration is 0.5-0.6% points (temperature difference = 10°C); (4) heat integration is less attractive when the temperature difference is larger than 40°C since the modified compression work is close to the actual work consumption without heat integration; (5) the optimal compression scheme does not save much power compared to adiabatic compression, thus adiabatic compression may be the most favorable when both investment cost and reliability are taken into consideration. The objective of this paper has been to investigate the maximum improvement potential in thermal efficiency by heat integration in oxy-combustion coal based power plants. Detailed heat exchanger network design and economic analysis are beyond the scope of the paper.

5.2. Thermodynamic analysis

Table A.1 in Appendix (the optimized case) shows that partial adiabatic compression has the lowest (modified) compression work. A comparison between "isothermal" compression and adiabatic compression (see Figure 6) from a thermodynamic point of view is helpful to understand the reason. Figure 5 shows that the initial and final states are fixed: (T_0 , p_0) and (T_F , p_F). The operating parameters in the dashed box are variables to be optimized. The energy balance can be formulated as shown by Eq. (10):

$$\dot{H}_F - \dot{H}_0 = (\dot{W}_1 + \dot{W}_2 + \dot{W}_3) - (\dot{Q}_1 + \dot{Q}_2 + \dot{Q}_3) - (\dot{Q}_{CW1} + \dot{Q}_{CW2} + \dot{Q}_{CW3}) \quad (10)$$

where $\dot{H}_0$ and $\dot{H}_F$ are the enthalpy of the air stream at initial and final states. $\dot{Q}_{CW1}$, $\dot{Q}_{CW2}$ and $\dot{Q}_{CW3}$ are the amounts of heat removed by cooling water after each compression stage. Since ($\dot{H}_F - \dot{H}_0$) is fixed, the RHS of Eq. (10) is also fixed. Assuming that two compression schemes are applied: "isothermal" compression and partial adiabatic compression (marked with single apostrophe), then Eq. (11) is satisfied.

$$(\dot{W}'_1+\dot{W}'_2+\dot{W}'_3)-(\dot{W}_1+\dot{W}_2+\dot{W}_3)=[(\dot{Q}'_1+\dot{Q}'_2+\dot{Q}'_3)-(\dot{Q}_1+\dot{Q}_2+\dot{Q}_3)]+ [(\dot{Q}'_{CW1}+\dot{Q}'_{CW2}+\dot{Q}'_{CW3})-(\dot{Q}_{CW1}+\dot{Q}_{CW2}+\dot{Q}_{CW3})] \quad (11)$$

Eq. (11) shows that all the increased work consumption due to adiabatic compression is converted into two portions of heat: one is transferred into the steam cycle and another is removed by CW. When adiabatic compression is applied, the amount of heat removed by the CW can be reduced, e.g. in the case of complete adiabatic compression, only one water cooler ("CW3" in Figure 5) is used. More heat can thus be transferred to the steam cycle for two reasons: (1) more compression work is consumed and (2) less heat is removed by CW. In addition, the heat transferred to the steam cycle can be upgraded to higher temperatures due to adiabatic compression.

6 Conclusions

Regenerative boiler feedwater preheating increases the thermal efficiency of steam Rankine cycles. When process heat is available for the preheating, less steam is extracted for preheating and more power is generated in the steam turbines. In oxy-combustion coal based power plants, considerable compression heat is available from the air separation unit, and this heat can be upgraded by using adiabatic compression. In addition, more heat is available for heat integration due to the increased compression work with adiabatic operation. This means that both the amount and quality of heat available for integration with the steam cycle is increased. How to integrate a heat stream with the steam cycle is also a challenge.

An MINLP model has been developed to investigate the optimal integration of the air compression train in a cryogenic air separation unit with the regenerative steam cycle in an oxy-combustion coal based power plant. Case studies and sensitivity analyses are performed to investigate the influence of temperature differences in heat exchangers and compressor efficiencies on heat integration. The thermal efficiency increases by a maximum of 0.4% points when "isothermal" compression is applied, and by a further 0.2% points when the compression scheme is optimized. Heat integration is less attractive when the temperature differences of the gas/water heat exchangers are larger than 40ºC. Adiabatic compression seems promising when investment cost is considered, however, further studies including economic analysis are required.

Acknowledgments

This publication has been produced with support from the BIGCCS Centre, performed under the Norwegian research program Centres for Environment-friendly Energy Research (FME). The authors acknowledge the following partners for their contributions: ConocoPhillips, Gassco, Shell, Statoil, TOTAL, GDF SUEZ and the Research Council of Norway (193816/S60).

Nomenclature

a	lower bound for the range of modified supply temperature
b	upper bound for the range of modified supply temperature
c	lower bound for the range of modified target temperature
$\overline{c}_p$	mean specific heat capacity, kJ/(kg·K)

d	upper bound for the range of modified target temperature
$DT_{\min}$	existing minimum temperature difference for heat transfer between steam and BFW, K or ^{o}C
$\Delta T_{\min}$	Minimum temperature difference for heat transfer between compressed air and BFW, K or ^{o}C
$\dot{H}$	enthalpy, kW
i	index for feedwater heater
j	index for temperature range
k	index for compression stage or heat stream
l	index for feedwater heater
n_h^L	lower bound for $T_{kT}^{'} - c_h$
N_h^L	upper bound for $T_{kT}^{'} - c_h$
m_g^L	lower bound for $T_{kS}^{'} - a_g$
M_g^L	upper bound for $T_{kS}^{'} - a_g$
$\dot{m}$	mass flow, kg/s
p	pressure, bar
$\dot{Q}$	heat, kW
r	index for feedwater heater
T	temperature, K or ^{o}C
n_h^U	lower bound for $T_{kT}^{'} - d_h$
N_h^U	upper bound for $T_{kT}^{'} - d_h$
m_g^U	lower bound for $T_{kS}^{'} - b_g$
M_g^U	upper bound for $T_{kS}^{'} - b_g$
$\dot{W}$	work, kW
X_k	upper bound for $T_{kT} - T_{kF}$
y	binary variable
Y_k	upper bound for $T_{kS} - T_{kT}$

Greek Letters

α	compression ratio
β	specific power reduction, kW/(kg/s)
γ	specific heat capacity ratio

Δ	symbol of differences
ε	small tolerance value
η	isentropic compressor efficiency
λ	binary variable
μ	binary variable
ξ	small tolerance value
π	binary variable
ρ	small tolerance value
σ	small tolerance value
ω	binary variable

Sub and superscripts

CW	cooling water
F	final
g	index for range of modified supply temperature
h	index for range of modified target temperature
i	index for feedwater heater
j	index for combined range for modified supply and target temperatures
k	index for compression stage or heat stream
L	lower bound for the range of modified supply or target temperature
max	maximum
min	minimum
S	supply
T	target
t	integer variable
U	upper bound for the range of modified supply or target temperature
'	modified; partial adiabatic compression
0	ambient condition

Abbreviations

ASU	air separation unit

BFW	boiler feedwater
CPU	CO_2 compression and purification unit
CW	cooling water
EOS	equation of state
ESP	electrostatic precipitator
FGD	flue gas desulfurization
FWH	feedwater heater
HE	heat exchanger
HHV	higher heating value
HP	higher pressure
IP	intermediate pressure
LP	lower pressure
MINLP	mixed integer nonlinear programming
PR	Peng-Robinson
RFG	recycled flue gas
RHS	right hand side
RKS	Redlich-Kwong-Soave
TTD	terminal temperature difference

Appendix

References

[1] Haywood RW. Analysis of engineering cycles: power, refrigerating and gas liquefaction plant. 4th ed. Oxford, England: Pergamon Press; 1991.
[2] Spliethoff H. Power generation from solid fuels. Berlin, Heidelberg, Germany: Springer-Verlag Berlin Heidelberg; 2010.
[3] Yan Q, Yang Y, Nishimura A, Kouzani A, Hu E. Multi-point and multi-level solar integration into a conventional coal-fired power plant. Energy & Fuels. 2010;24(7):3733-8.
[4] Bruhn M. Hybrid geothermal-fossil electricity generation from low enthalpy geothermal resources: geothermal feedwater preheating in conventional power plants. Energy. 2002;27(4):329-46.
[5] Luo X, Zhang B, Chen Y, Mo S. Heat integration of regenerative Rankine cycle and process surplus heat through graphical targeting and mathematical modeling technique. Energy. 2012;45(1):556-69.
[6] Romeo LM, Bolea I, Lara Y, Escosa JM. Optimization of intercooling compression in CO_2 capture systems. Applied Thermal Engineering. 2009;29(8-9):1744-51.

[7] Fu C, Gundersen T. Exergy analysis and heat integration of a coal-based oxy-combustion power plant. Energy & Fuels. 2013;27(11):7138-49.
[8] Fu C, Gundersen T. Integrating the compression heat in oxy-combustion power plants with CO_2 capture. Chemical Engineering Transactions. 2012;29:781-6.
[9] DOE/NETL. Advanced carbon dioxide capture R&D program: technology update. May 2013.
[10] Higginbotham P, White V, Fogash K, Guvelioglu G. Oxygen supply for oxyfuel CO_2 capture. International Journal of Greenhouse Gas Control. 2011;5, Supplement 1:S194-S203.
[11] Fu C, Gundersen T. Using exergy analysis to reduce power consumption in air separation units for oxy-combustion processes. Energy. 2012;44(1):60-8.
[12] Smith R. Chemical process design and integration. Hoboken, New Jersey, US: John Wiley and Sons, Ltd.; 2005.
[13] Fu C, Anantharaman R, Gundersen T. Optimal integration of compression heat with regenerative steam Rankine cycles. Computer Aided Chemical Engineering. 2014;34:519-24.
[14] DOE/NETL. Pulverized coal oxycombustion power plants. Washington, D.C.: DOE/NETL; 2008, 2007/1291.
[15] STEAM PRO 21.0, 2012. Help document. www.thermoflow.com.
[16] El-Wakil MM. Powerplant technology. New York, US: McGraw-Hill; 2002.
[17] Williams HP. Model building in mathematical programming. 5th ed. Chichester, UK: John Wiley and Sons Ltd.; 2013.
[18] Knapp H, Doring R, Oellrich L, Plocker U, Prausnitz JM. Vapor-liquid equilibria for mixtures of low boiling substances. DECHEMA Chemistry Sries VI. Frankfurt, Germany, 1982.
[19] Rosenthal RE. GAMS - A user's guide. GAMS Development Corporation, Washington, D.C., USA: 2013.

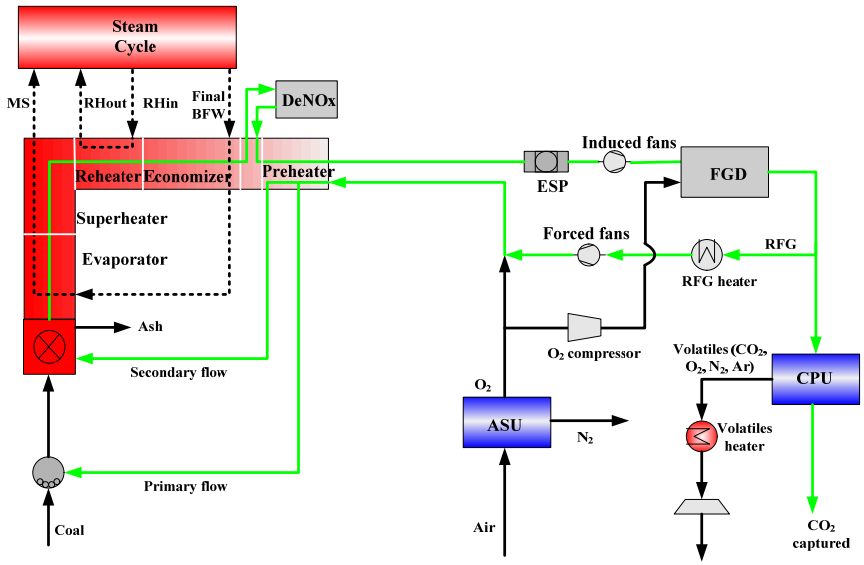

Figure 1 The coal based oxy-combustion power plant with CO_2 capture

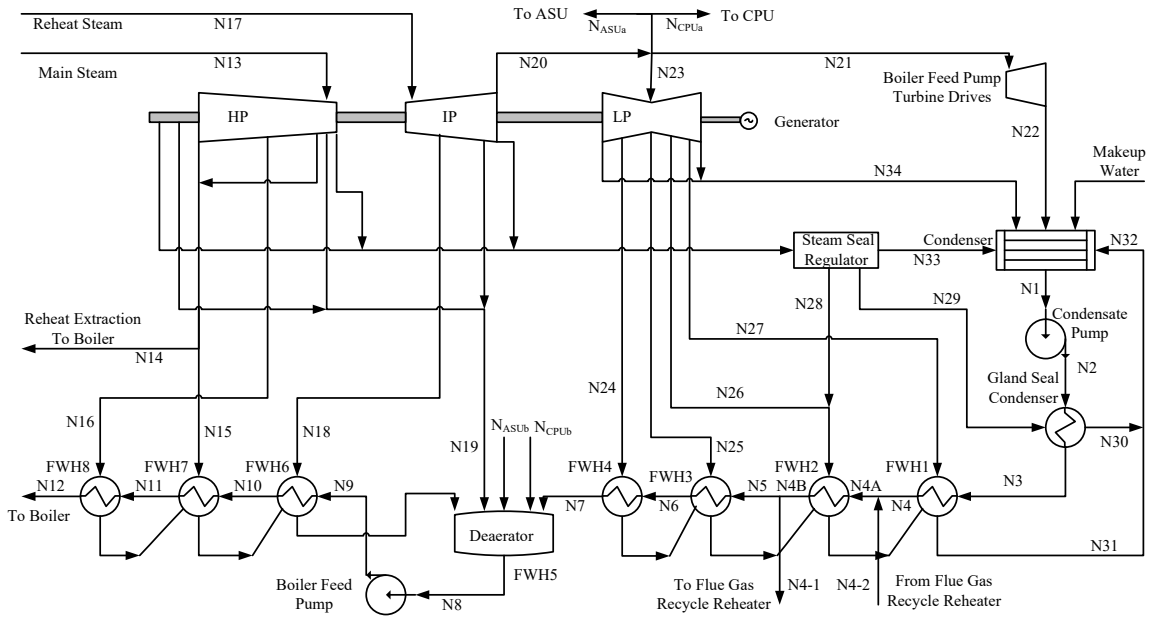

Figure 2 The reference steam cycle

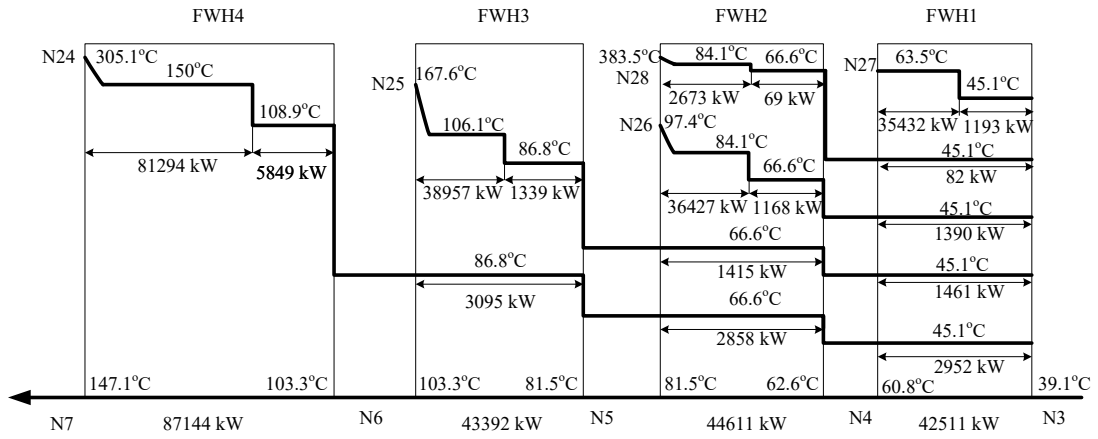

(a)

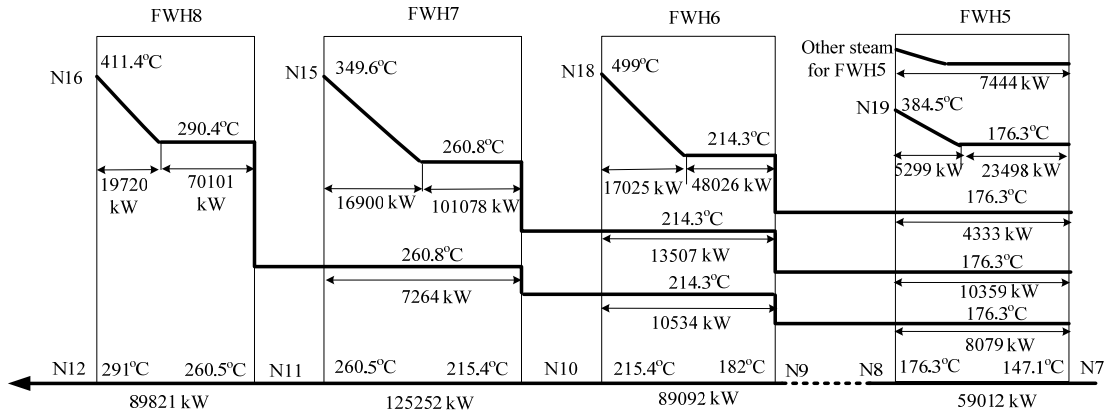

(b)

Figure 3 Decomposed heat loads in the FWHs: (a) FWH1-4; (b) FWH5-8

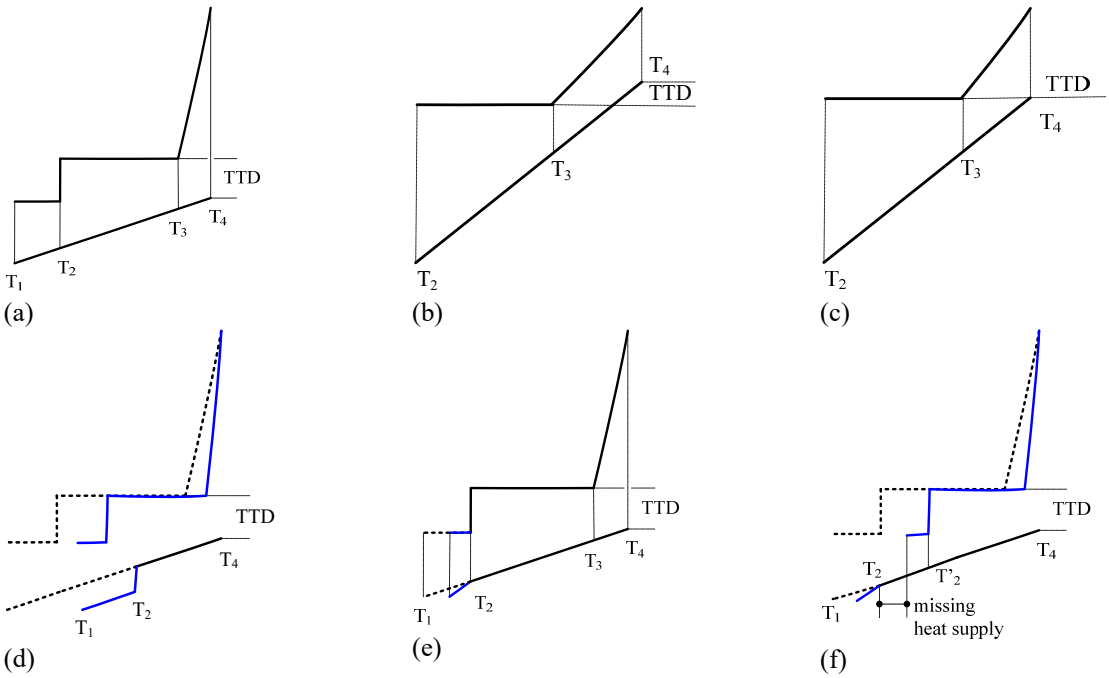

Figure 4 Temperature profiles for different FWH configurations: (a) LP FWHs; (b) HP FWHs; (c) Deaerator; (d) Appropriate heat integration with LP FWHs; (e) Inappropriate heat integration with LP FWHs; (f) Unbalanced curves in the LP FWHs

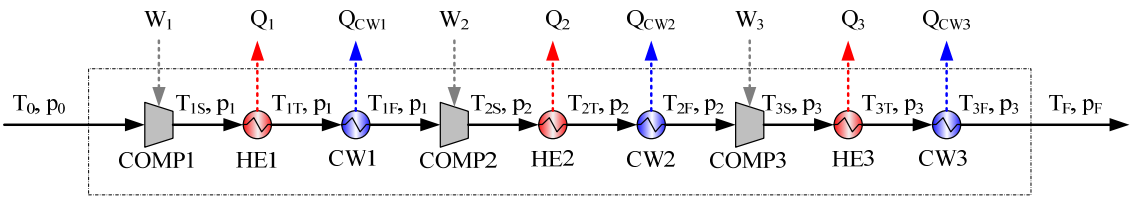

Figure 5 The compression scheme

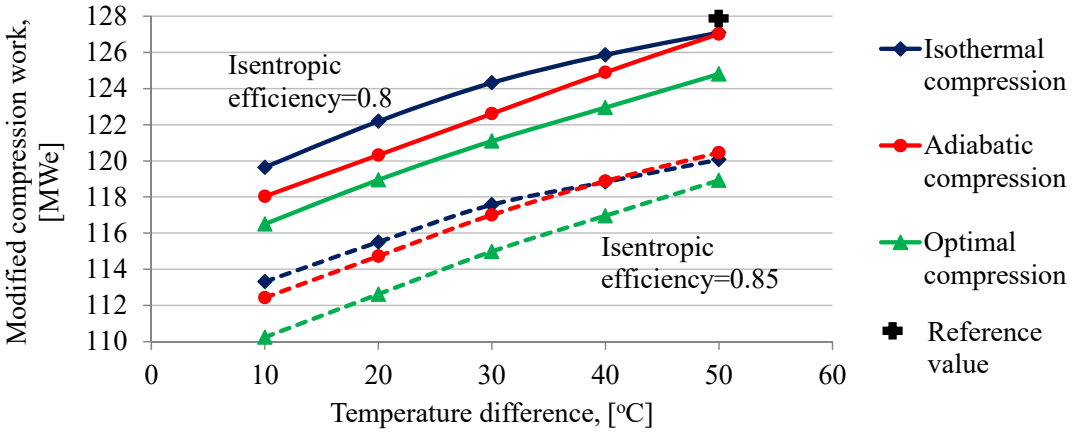

Figure 6 Performance of the heat integration

Table 1 Characteristics of extracted steam in the reference steam cycle

Steam	Mass flow, kg/s	Heat contribution, kW	Power reduction, kW	Specific power reduction, β, kW/(kg/s)
N15	60.995	141,844	61,282	1004.71
N16	47.570	115,698	52,911	1112.28
N18	25.515	69,384	24,326	953.40
N19	11.591	28,797	8,378	722.80
N24	33.281	96,048	22,065	663.00
N25	16.477	43,172	6,628	402.26
N26	15.674	38,985	4,260	271.79
N27	15.481	36,625	2,362	152.57

Table 2 Criteria for heat integration

	Main features	Integration is performed when
LP FWHs	$DT_{\min} \approx$ TTD	$T_2 \le T'_{kS} < T_4$ or $T_2 \le T'_{kT} < T_4$
HP FWHs	TTD < 0 K	$T_3 \le T'_{kS} < T_4$ or $T_3 \le T'_{kT} < T_4$
Deaerator	TTD = 0 K	$T_2 \le T'_{kS} < T_4$ or $T_2 \le T'_{kT} < T_4$

Table 3 Temperature ranges for heat integration in the reference steam cycle

T'_{kS} (°C)			g =1	g =2	g =3	g =4	g =5	g =6	g =7
			FWH1	FWH2	FWH3	FWH4	FWH5	FWH6	FWH7
			[42.7, 64.9)	[64.9, 83.7)	[83.7, 106.2)	[106.2, 147.1)	[147.1, 209)	[209, 254.4)	[254.4, T'_{max})
T'_{kT} (°C)	h =1	FWH1	[42.7, 64.9)	[42.7, 64.9)	[42.7, 64.9)	[42.7, 64.9)	[42.7, 64.9)	[42.7, 64.9)	[42.7, 64.9)
	h =2	FWH2	-	[64.9, 83.7)	[64.9, 83.7)	[64.9, 83.7)	[64.9, 83.7)	[64.9, 83.7)	[64.9, 83.7)
	h =3	FWH3	-	-	[83.7, 106.2)	[83.7, 106.2)	[83.7, 106.2)	[83.7, 106.2)	[83.7, 106.2)
	h =4	FWH4	-	-	-	[106.2, 147.1)	[106.2, 147.1)	[106.2, 147.1)	[106.2, 147.1)
	h =5	FWH5	-	-	-	-	[147.1, 209)	[147.1, 209)	[147.1, 209)
	h =6	FWH6	-	-	-	-	-	[209, 254.4)	[209, 254.4)
	h =7	FWH7	-	-	-	-	-	-	[254.4, T'_{max})

Table 4 Comparison of the PR model and the ideal gas model for the compression of air

Pressure ratio	PR model		Ideal gas model		Relative difference, %	
	temperature, K	enthalpy, kJ/kg	temperature, K	enthalpy, kJ/kg	temperature	enthalpy
2	363.40	65.24	363.34	65.54	-0.018	0.458
3	407.77	110.04	407.65	110.33	-0.029	0.258
4	442.32	145.11	442.16	145.37	-0.037	0.175
5	470.98	174.36	470.78	174.57	-0.043	0.123
6	495.66	199.66	495.42	199.83	-0.049	0.084

Table A.1 Stream data for the reference steam cycle

Stream	p, bar	T, K	$\dot{m}$, kg/s
N1	0.07	311.5	467.853
N2	17.24	311.7	467.853
N3	16.89	312.2	467.853
N4	16.55	334.0	467.853
N4-1	15.86	354.6	97.014
N4-2	16.55	344.3	97.014
N4A	16.55	335.7	564.867
N4B	15.86	354.6	564.867
N5	15.86	354.6	467.853
N6	15.51	376.7	467.853
N7	15.17	420.4	467.853
N8	9.21	449.5	612.787
N9	289.58	455.1	612.787
N10	289.24	488.5	612.787
N11	288.89	533.6	612.787
N12	288.55	564.1	612.787
N13	242.33	872.0	612.787
N14	49.01	624.2	500.354
N15	47.54	622.8	60.995
N16	74.81	684.6	47.570
N17	45.22	894.3	500.354
N18	20.74	773.1	25.515
N19	9.21	654.0	11.591
N20	9.49	657.7	462.301
N21	9.49	657.7	36.304
N23	9.49	657.7	423.729
N24	4.76	578.3	33.281
N25	1.25	440.7	16.477
N26	0.56	370.5	15.674
N27	0.23	336.7	15.481
N28	0.56	656.6	0.924
N29	1.01	657.0	0.352
N30	1.01	373.2	0.352
Makeup water	1.01	298.1	6.128

Table A.2 Results of optimized compression scheme

$\Delta T_{\min}$, °C		Isentropic efficiency = 0.80			Isentropic efficiency = 0.85		
		Stage1	Stage2	Stage3	Stage1	Stage2	Stage3
10	Outlet pressure, bar	3.68	5.05	5.6	3.95	4.7	5.6
	T_{kS}, °C	188	136.1	130.5	188.5	139	139.1
	T_{kT}, °C	93.6	116.2	52.7	116.1	116.1	52.7
	T_{kF}, °C	93.6	116.2	35	116.1	116.1	35
	$\dot{m}_{i,k}^{steam,new}$, kg/s						
	FWH1 (N27)	16.043	15.651	9.999	15.83	15.676	10.072
	FWH2 (N26)	16.203	15.842	10.99	16.02	15.868	11.062
	FWH3 (N25)	10.971	16.662	10.723	16.831	16.663	10.803
	FWH4 (N24)	23.287	28.418	29.792	23.287	27.7	27.695
	FWH5 (N19)	3.636	11.591	11.591	3.513	11.591	11.591
	FWH6 (N18)	25.515	25.515	25.515	25.515	25.515	25.515
	FWH7 (N15)	60.995	60.995	60.995	60.995	60.995	60.995
	Compression work, kW			140680			134023
	Increased turbine power, kW			24177			23782
	Modified compression work, kW			116503			110241
20	Outlet pressure, bar	4.31	5.24	5.6	4.2	4.84	5.6
	T_{kS}, °C	212.1	154.5	70.4	197.2	145.5	145.5
	T_{kT}, °C	126.2	62.7	62.7	126.1	126.1	62.7
	T_{kF}, °C	126.2	62.7	35	126.1	126.1	35
	$\dot{m}_{i,k}^{steam,new}$, kg/s						
	FWH1 (N27)	15.829	10.118	13.397	15.83	15.646	10.042
	FWH2 (N26)	16.019	11.108	15.674	16.02	15.838	11.033
	FWH3 (N25)	16.857	10.854	16.477	16.831	16.63	10.77
	FWH4 (N24)	23.287	26.37	33.281	23.287	28.57	28.566
	FWH5 (N19)	0	11.591	11.591	3.83	11.591	11.591
	FWH6 (N18)	25.515	25.515	25.515	25.515	25.515	25.515
	FWH7 (N15)	60.995	60.995	60.995	60.995	60.995	60.995
	Compression work, kW			142873			135076
	Increased turbine power, kW			23925			22451
	Modified compression work, kW			118948			112625
30	Outlet pressure, bar	4.59	4.59	5.6	1.01	4.65	5.6
	T_{kS}, °C	222.1	72.7	57.1	25	212.7	54.3
	T_{kT}, °C	72.7	72.7	57.1	25	72.7	54.3
	T_{kF}, °C	72.7	35	35	25	35	35
	$\dot{m}_{i,k}^{steam,new}$, kg/s						
	FWH1 (N27)	10.226	15.481	15.481	15.481	10.226	15.481
	FWH2 (N26)	11.214	15.674	15.674	15.674	11.214	15.674
	FWH3 (N25)	10.971	16.477	16.477	16.477	10.971	16.477
	FWH4 (N24)	23.287	33.281	33.281	33.281	23.287	33.281
	FWH5 (N19)	0	11.591	11.591	11.591	2.412	11.591
	FWH6 (N18)	25.515	25.515	25.515	25.515	25.515	25.515

	FWH7 (N15)	60.995	60.995	60.995	60.995	60.995	60.995
	Compression work, kW			140325			132478
	Increased turbine power, kW			19233			17490
	Modified compression work, kW			121092			114988
40	Outlet pressure, bar	4.65	4.65	5.6	1.29	1.45	5.6
	T_{kS} , ºC	224.5	187.1	55.5	49.5	47.8	201.7
	T_{kT} , ºC	187.1	82.7	55.5	49.5	47.8	82.7
	T_{kF} , ºC	187.1	35	35	35	35	35
	$\dot{m}_{i,k}^{steam,new}$, kg/s						
	FWH1 (N27)	15.481	10.226	15.481	15.481	15.481	10.226
	FWH2 (N26)	15.674	11.214	15.674	15.674	15.674	11.214
	FWH3 (N25)	16.477	10.971	16.477	16.477	16.477	10.971
	FWH4 (N24)	33.281	23.287	33.281	33.281	33.281	23.287
	FWH5 (N19)	1.965	11.591	11.591	11.591	11.591	7.82
	FWH6 (N18)	25.515	25.515	25.515	25.515	25.515	25.515
	FWH7 (N15)	60.995	60.995	60.995	60.995	60.995	60.995
	Compression work, kW			140758			130545
	Increased turbine power, kW			17812			13581
	Modified compression work, kW			122946			116964
50	Outlet pressure, bar	4.65	4.65	5.6	4.13	4.13	5.6
	T_{kS} , ºC	224.5	224.5	55.5	195	114.9	67.3
	T_{kT} , ºC	224.5	92.7	55.5	114.9	92.7	67.3
	T_{kF} , ºC	224.5	35	35	114.9	35	35
	$\dot{m}_{i,k}^{steam,new}$, kg/s						
	FWH1 (N27)	15.481	10.226	15.481	16.212	9.477	15.481
	FWH2 (N26)	15.674	11.214	15.674	11.197	15.674	15.674
	FWH3 (N25)	16.477	10.971	16.477	10.951	16.477	16.477
	FWH4 (N24)	33.281	23.287	33.281	23.803	33.281	33.281
	FWH5 (N19)	11.591	4.541	11.591	11.591	11.591	11.591
	FWH6 (N18)	25.515	25.515	25.515	25.515	25.515	25.515
	FWH7 (N15)	60.995	60.995	60.995	60.995	60.995	60.995
	Compression work, kW			140758			129448
	Increased turbine power, kW			15951			10528
	Modified compression work, kW			124807			118920